Supporting Information

Unraveling the effect of transition-metal doping on the structural, electronic, and electrocatalytic HER performance of monolayer $HfTe_2$

Panxing Liao,[†abc] Yanshan Li,[†ac] Yifan Wang,[ac] Qingyun Yang,[ac] Wen Wang,[ac] Meiqi Chen,[ac] Cai Cheng[*ac] Ling Li,[ac] and Ke Liu[*ac]

[a] Key Laboratory of Micro-Nano Optoelectronic Materials and Devices at Sichuan Normal University of Sichuan Province, Chengdu 610101, China

[b] School of Intelligent Manufacturing, Nanning University, Nanning 530200, China

[c] School of Physics and Electronic Engineering, Sichuan Normal University, Chengdu 610101, China

† Panxing Liao and Yanshan Li contributed equally to this work and they should be regarded as co-first authors.

*Corresponding author E-mails: ccheng@sicnu.edu.cn; lkworld@sicnu.edu.cn

S1. Cutoff energy and the *k*-point grid convergence test

Convergence tests were performed to determine suitable parameters for monolayer $HfTe_2$ calculations. The plane-wave cutoff energy (ENCUT) was tested from 400 to 500 eV while keeping the *k*-point grid fixed at 4×4×1. Separately, the *k*-point grid was tested from 4×4×1 to 6×6×2 with ENCUT fixed at 400 eV. The results (Table S1) show that the total energy changes are less than 0.01 eV, confirming sufficient convergence. Based on these tests, a 400 eV cutoff energy and a 4×4×1 *k*-point grid were adopted for all monolayer calculations to balance accuracy and computational cost.

Table S1. Cutoff energy and the *k*-point grid test for monolayer $HfTe_2$.

Test	Parameters	Total Energy (eV)	Relative Difference (%)
Cutoff energy (*k*-point: 4×4×1)	ENCUT = 400 eV	–299.82407	Reference
	ENCUT = 500 eV	–299.82902	0.00165
k-point grid (ENCUT =400 eV)	*k*-point = 4×4×1	–299.82407	Reference
	k-point = 6×6×2	–299.81436	0.00324

S2. Stability of pristine and TM-doped $HfTe_2$ structures

S2.1 Ab Initio molecular dynamics (AIMD) simulations

AIMD simulations were performed in the NVT ensemble at 300 K using the Nosé-Hoover thermostat. For pristine bulk and monolayer structures, a 5 ps simulation with a 2.5 fs time step was used; for H-adsorbed structures, a 3 ps simulation with a 3 fs time step was adopted. The results (Figs. S1 and S2) show that the total energy fluctuates around a stable average and no bond breaking or structural reconstruction occurs, confirming the thermodynamic stability of these systems at room temperature.

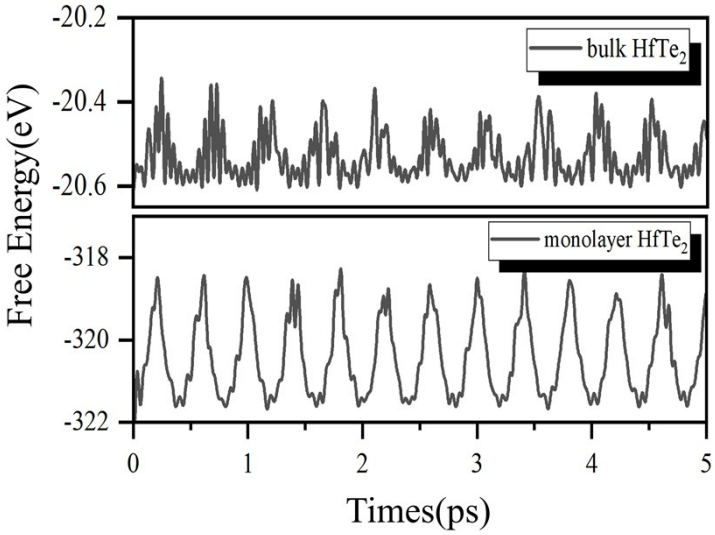

Fig. S1. Energy fluctuation during AIMD simulations at 300 K for (a) bulk $HfTe_2$ and (b) monolayer $HfTe_2$ supercell.

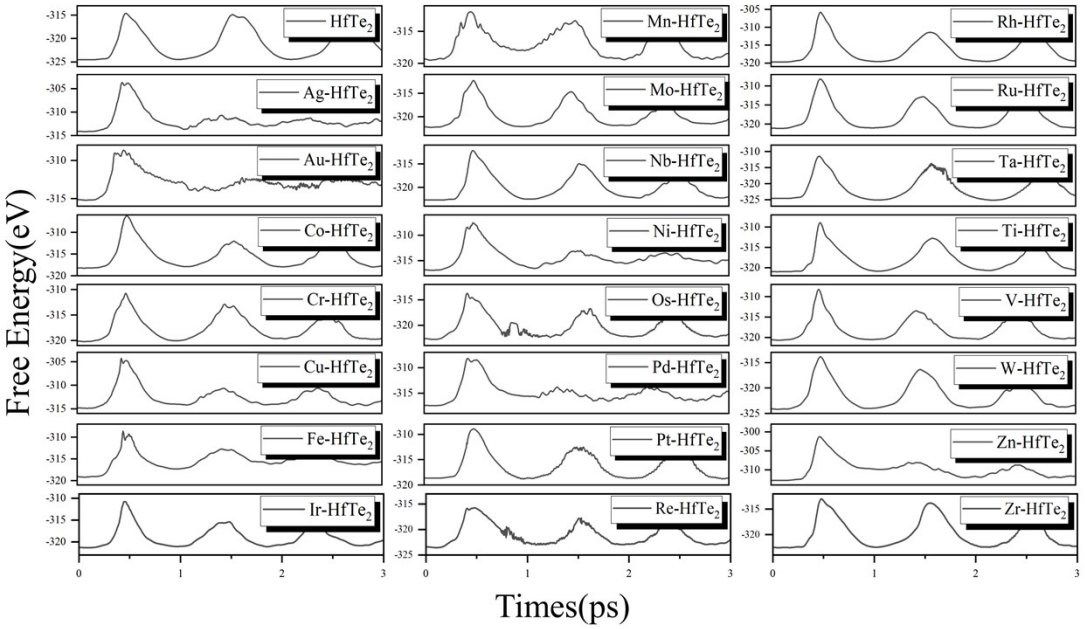

Fig. S2. Energy fluctuation during AIMD simulations at 300 K for H-adsorbed structures on pristine $HfTe_2$ and TM-doped $HfTe_2$ surfaces.

S2.2 Phonon spectra

Phonon spectra of bulk and monolayer $HfTe_2$ supercell (size was 2×2×1) are shown in Fig. S3. The phonon spectra of the H adsorption structure of undoped and doped $HfTe_2$ are shown in the Fig. S4. No imaginary frequencies are present in the entire Brillouin zone, confirming dynamical stability. The small imaginary frequency near the *G* point is caused by the fact that the phonopy used in the phonon calculation only considers translation invariance without considering rotation invariance, which is more common in the calculation of 2D materials.

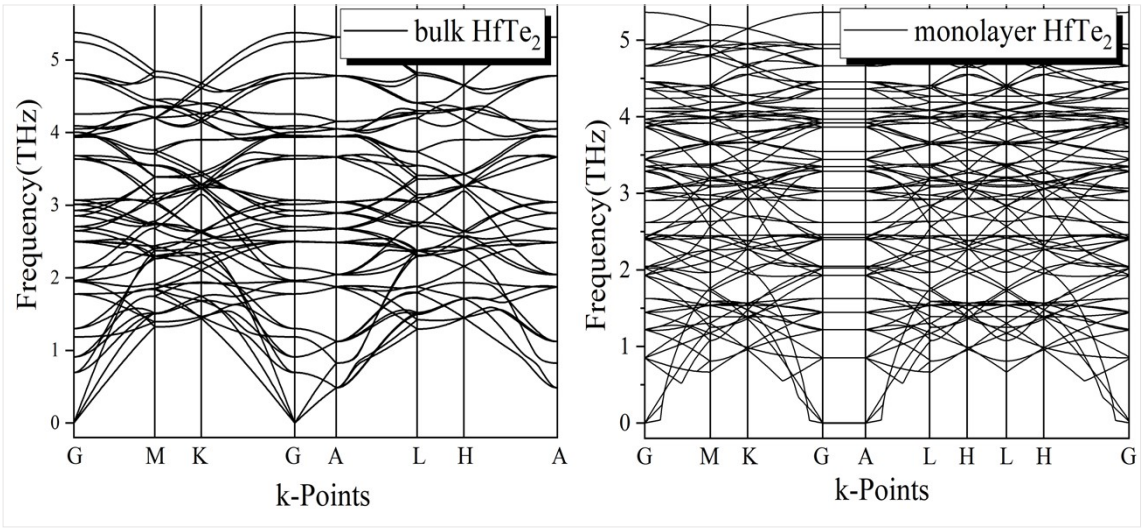

Fig. S3. Phonon spectra of bulk and monolayer $HfTe_2$.

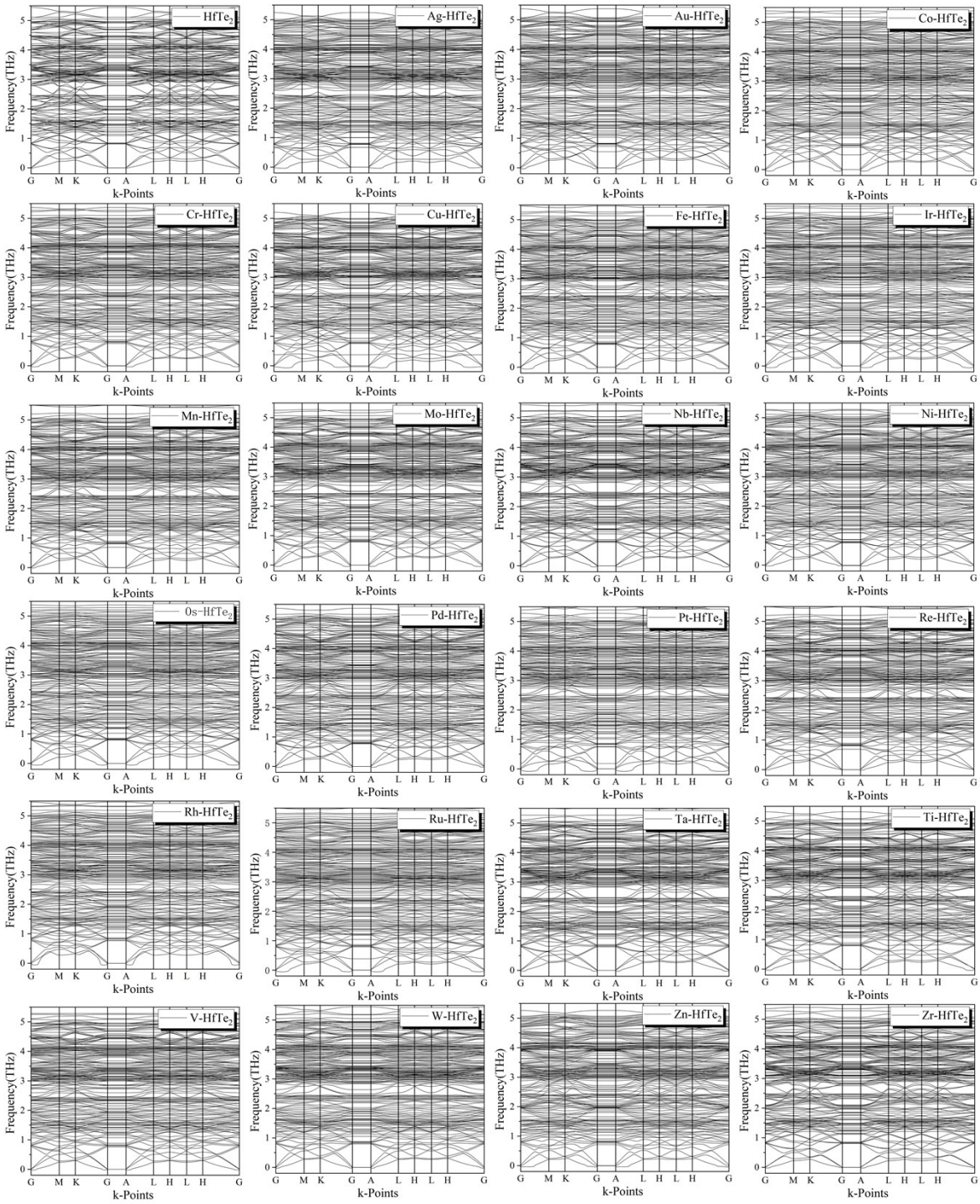

Fig. S4. Phonon spectra of the hydrogen adsorption structure of pristine and TM-doped $HfTe_2$.

S2.3 Formation energies of doped systems

The substitutional formation energy (ΔE_{form}) for a doped system $Te_{32}Hf_{15}X_1$ (X = dopant) under Te-rich growth conditions is calculated as:

$$\Delta E_{\text{form}}(\mu) = E_{(\text{Te}_{32}\text{Hf}_{15}X_1)} - E_{(\text{Te}_{32}\text{Hf}_{16})} + \mu_{\text{Hf}}^{\text{Te-rich}} - \mu_X \quad (1)$$

Where E denotes the total energy of the system, and μ_X is the chemical potential of the dopant (taken as the energy per atom in its pure metal bulk), and $\mu_{\text{Hf}}^{\text{Te-rich}}$ is the chemical potential of Hf under Te-rich conditions.

For $HfTe_2$, the chemical potentials of Hf and Te are constrained by the phase stability condition:

$$\mu_{\text{Hf}} + 2\mu_{\text{Te}} = \mu_{\text{HfTe}_2} \quad (2)$$

Under Te-rich growth conditions, the chemical potential of Te reaches its maximum ($\mu_{\text{Te}} = \mu_{\text{Te}}^0$, the energy of bulk Te), which determines μ_{Hf}:

$$\mu_{\text{Hf}}^{\text{Te-rich}} = \mu_{\text{HfTe}_2} - 2\mu_{\text{Te}}^0 \quad (3)$$

Using our DFT-calculated chemical potentials (μ_{HfTe_2} =−18.6882 eV, μ_{Te}^0 =−3.1423 eV, μ_{Hf}^0 = −9.9246 eV), we obtain:

$$\mu_{\text{Hf}}^{\text{Te-rich}} = -18.6882 - 2\times(-3.1423) = -12.4036 \ \text{eV}.$$

Table S2 presents the formation energies under Te-rich growth conditions. The results show that under Te-rich conditions—the most favorable for $HfTe_2$ growth—the formation energies of all 23 dopants become negative, confirming the thermodynamic feasibility of doping.

Table S2. Formation energies of TM-doped $HfTe_2$ systems under Te-rich growth conditions.

Dopant(X)	$E_{(\text{Te32Hf15X1})}$ (eV)	Te-rich ΔE_{form} (eV)	Dopant(X)	$E_{(\text{Te32Hf15X1})}$ (eV)	Te-rich ΔE_{form} (eV)	Dopant(X)	$E_{(\text{Te32Hf15X1})}$ (eV)	Te-rich ΔE_{form} (eV)
/	-39.6629	/	Cu	-35.9346	–8.6753	Ag	-38.4715	–11.2122
Ti	-38.8853	–11.6260	Zn	-36.6969	–9.4376	Ta	-37.763	–10.5037
V	-37.1586	–9.8993	Zr	-39.7424	–12.4831	W	-36.0444	–8.7851
Cr	-35.9656	–8.7063	Nb	-38.1277	–10.8684	Re	-33.9108	–6.6515
Mn	-36.367	–9.1077	Mo	-36.6595	–9.4002	Os	-34.5616	–7.3023
Fe	-35.6968	–8.4375	Ru	-36.5127	–9.2534	Ir	-36.1612	–8.9019
Co	-35.9843	–8.7250	Rh	-37.2931	–10.0338	Pt	-37.1567	–9.8974
Ni	-36.1447	–8.8854	Pd	-37.1283	–9.8690	Au	-36.2176	–8.9583

Note: $\mu_{\text{Hf}}^{\text{Te-rich}}$ =-12.4036, derived from μ_{HfTe_2} =−18.6882 eV and μ_{Te}^0 =−3.1423 eV.

S3. Complete electronic structure data

For clarity, the main text presents the projected density of states (PDOS) and the total density of states (TDOS） of undoped and TM-doped $HfTe_2$ only for the six most promising dopants (Fe, Co, Ru, Re, Ir, and Au). The complete set of PDOS and total density of states (TDOS) for the pristine and all 23 doped systems is provided in Fig. S5.

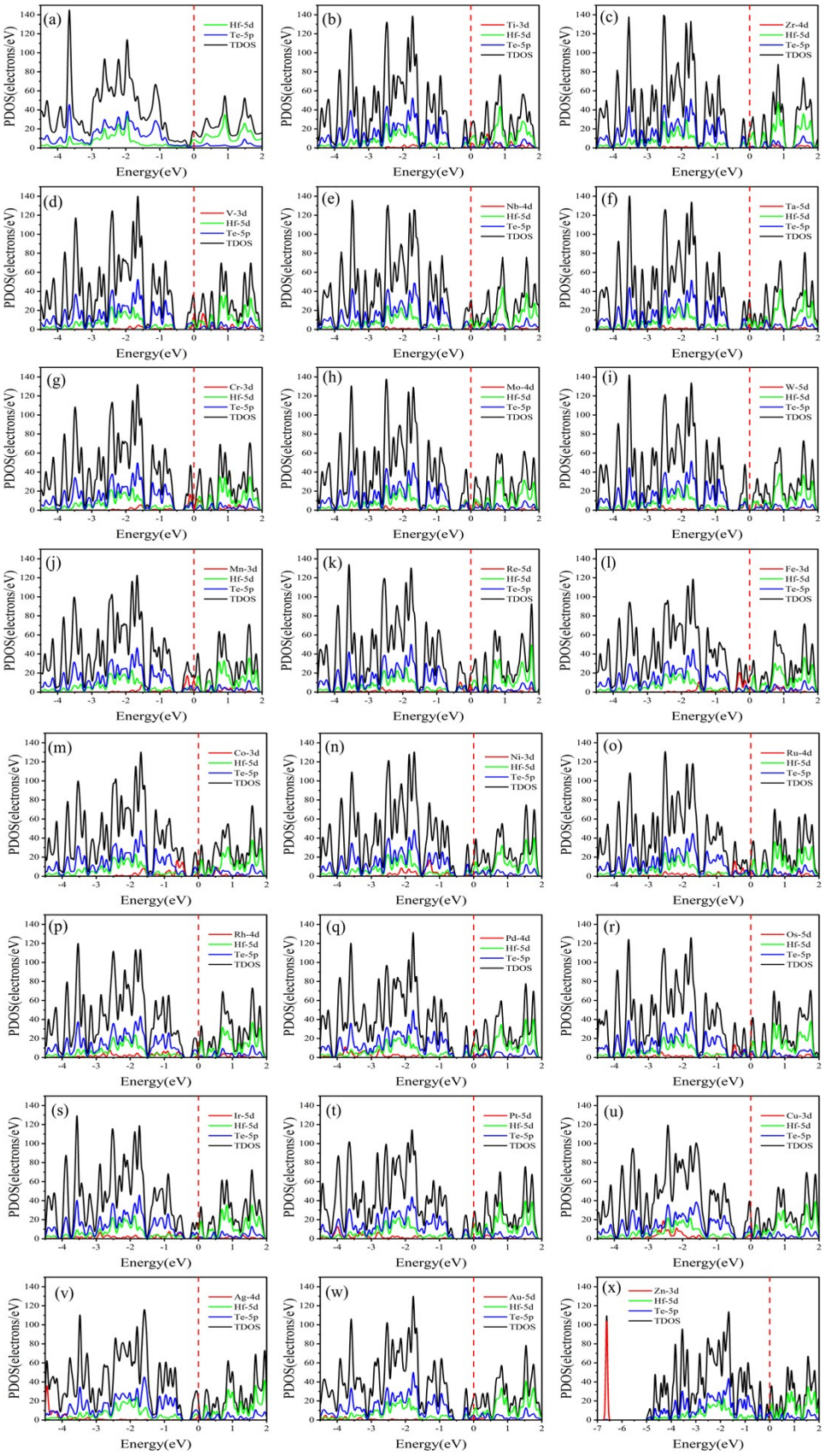

Fig. S5. PDOS and TDOS of pristine and TM-doped $HfTe_2$.

S4. Complete geometrical structures of hydrogen adsorption

The main text shows the local side view of the optimized H adsorption structures for the six key doped systems and the pristine surface. The complete set of local side views for all 23 doped systems is provided in Fig. S6.

Fig. S6(a) shows H adsorption on the pristine surface, where H binds vertically to a surface Te atom. The Te-H

bond length is 1.687 Å. Upon H adsorption, the Hf-Te bond associated with the Te atom elongates from 2.891 Å to 2.942 Å, while the other two Hf-Te bonds shorten to 2.854 Å.

Fig. S6(b)–(x) show H adsorption on TM-doped surfaces. In all cases, the H atom adsorbs on a Te site adjacent to the dopant. The TM–Te bond associated with this Te atom is elongated, while the other two TM–Te bonds contract. Based on the magnitude of elongation, the systems can be divided into two groups:

1. For Zr, Mn, Ni, Pd, Cu, Ag, Au, and Zn dopants, the TM–Te(H) bond elongates significantly (0.02–0.76 Å), resulting in bond lengths between 2.96 and 3.71 Å.
2. For the remaining 15 dopants, the TM–Te(H) bond either shortens or shows only a slight elongation.

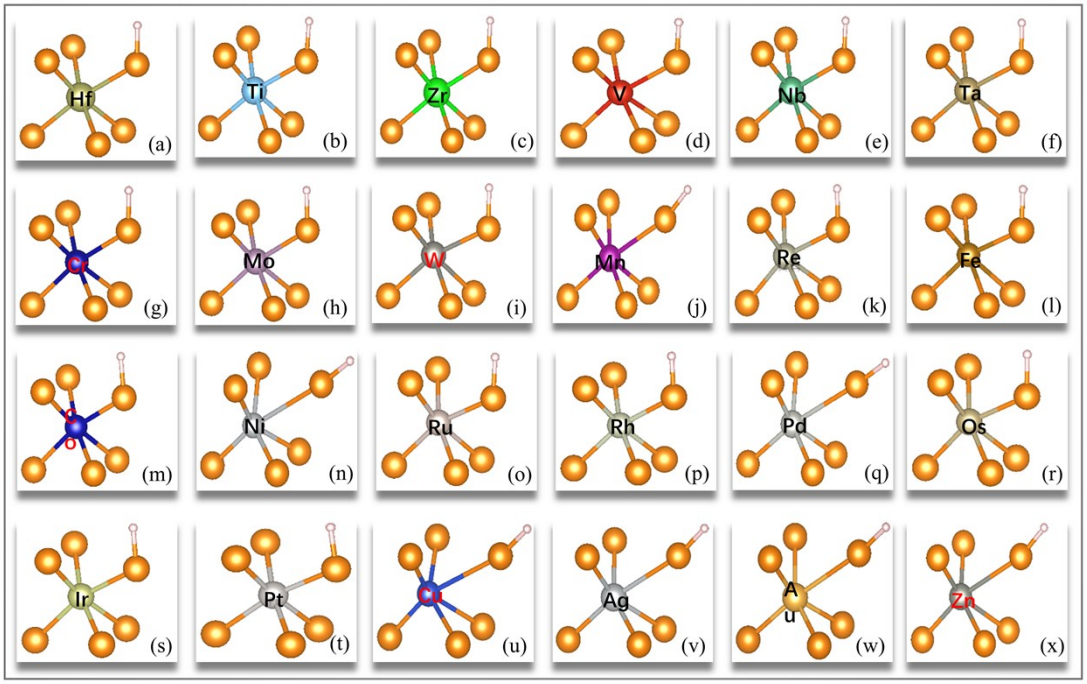

Fig. S6. Local side view of the optimized H adsorption structures on (a) pristine and (b-x) 23 different TM-doped $HfTe_2$ surfaces.

Table S3. Structural parameters after H adsorption: Te-H bond length (d_{Te-H}) and the corresponding TM-Te bond length ($d_{TM-Te(H)}$).

Dopant(*X*)	d_{Te-H}(Å)	$d_{TM-Te(H)}$(Å)	Dopant(*X*)	d_{Te-H}(Å)	$d_{TM-Te(H)}$(Å)
/	2.891	1.687	Mo	1.690	2.806
Ti	1.686	2.848	Ru	1.698	2.684
V	1.688	2.788	Rh	1.696	2.639
Cr	1.693	2.722	Pd	1.692	3.632
Mn	1.69	3.323	Ag	1.690	3.523
Fe	1.700	2.598	Ta	1.691	2.895
Co	1.698	2.55	W	1.695	2.814
Ni	1.688	3.706	Re	1.698	2.767
Cu	1.688	3.701	Os	1.695	2.716
Zn	1.684	3.475	Ir	1.696	2.660
Zr	1.683	2.962	Pt	1.697	2.650
Nb	1.688	2.890	Au	1.687	3.564

S5. Note on the computational hydrogen electrode model

All calculations of hydrogen adsorption free energy (ΔG_H) are based on the computational hydrogen electrode (CHE) model developed by Nørskov and coworkers[S1, S2]. In this standard model, the equilibrium potential for the

H^+/H_2 couple under standard conditions (pH = 0) is defined as 0 V versus the reversible hydrogen electrode (RHE). This provides a consistent thermodynamic reference for evaluating HER catalysts in acidic media and follows the established convention for theoretical HER studies.

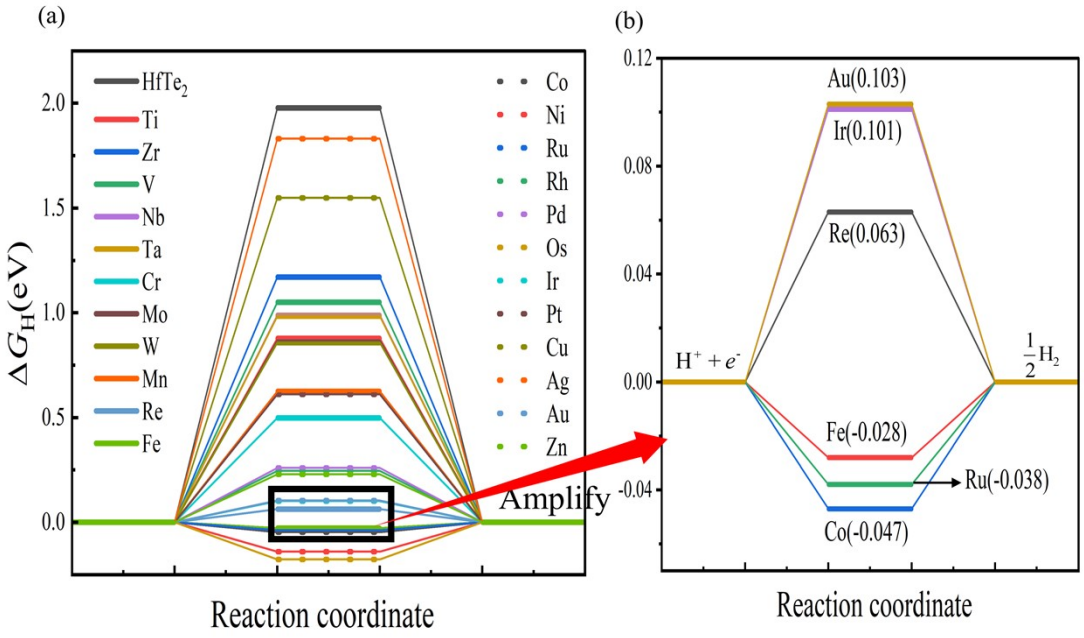

Fig. S7. Hydrogen adsorption Gibbs free energy (ΔG_H) of (a) monolayer $HfTe_2$ and $HfTe_2$ doped with different transition metals, and (b) a close-up view of several doping systems with ΔG_H close to zero.

S6. Energetic and electronic parameters for pristine and TM-doped monolayer $HfTe_2$.

Table S4. Key descriptors for pristine and TM-doped monolayer $HfTe_2$: d-band center (ε_d), hydrogen adsorption free energy (ΔG_H), and substitutional formation energy (ΔE_{form}).

Dopant(*X*)	ΔE_H(eV)[2]	ΔG_H(eV)	ε_d(eV)[1]	Dopant(*X*)	ΔE_H(eV)[2]	ΔG_H(eV)	ε_d(eV)[1]
/	2.942	1.754	-2.48	Mo	0.645	0.868	-2.08
Ti	0.657	0.878	-2.05	**Ru**	-0.263	**-0.038**	-2.08
Ti	0.657	0.878	-2.05	Rh	0.020	0.245	-2.06
Cr	0.274	0.498	-2.00	Pd	0.029	0.259	-2.07
Mn	0.401	0.625	-2.00	Ag	1.602	1.831	-2.42
Fe	-0.251	**-0.028**	-1.99	Ta	0.761	0.984	-2.10
Co	-0.270	**-0.047**	-1.93	W	0.632	0.857	-2.12
Ni	-0.370	-0.140	-1.95	**Re**	-0.162	**0.063**	-2.14
Cu	1.319	1.548	-2.36	Os	-0.404	-0.178	-2.10
Zn	-0.001	0.229	-2.45	**Ir**	-0.125	**0.101**	-2.17
Zr	0.948	1.170	-2.09	Pt	0.385	0.611	-2.11
Nb	0.765	0.987	-2.08	**Au**	-0.128	**0.103**	-2.21

Notes:

[1] The d-band center (ε_d) is calculated as the first moment of the projected density of states (PDOS) for the dopant's d-orbitals, relative to the Fermi level.

[2] Parameters: ΔE_H, hydrogen adsorption energy; ΔG_H, hydrogen adsorption free energy at standard conditions (pH=0, 298 K); ΔQ_{Te}, Bader charge change on the H-binding Te atom after doping (negative value indicates electron loss).

[3] **Bold** entries for ΔG_H highlight dopants with values closest to the ideal thermodynamic optimum ($\Delta G_H \approx 0$ eV).

S7. Dissolution potential calculations

To assess the electrochemical stability of the doped systems under operating conditions, we calculated the

dissolution potential (U_{diss}) for the key dopants following the standard method in electrocatalysis[S3, S4]. The dissolution potential indicates the thermodynamic tendency of the dopant to leach from the $HfTe_2$ lattice into the electrolyte.

The dissolution potential is calculated using the thermodynamic cycle:

$$U_{\text{diss}} = U^{\text{o}}(\text{M}^{\text{n+}}/\text{M}) - \frac{\Delta G_{\text{binding}}}{nF} \quad (2)$$

where:

- $U^{\text{o}}(\text{M}^{n+}/\text{M})$ is the standard electrode potential of the pure metal (taken from the CRC Handbook of Chemistry and Physics; for Ru and Re, values from Bard et al. [S5]
- $\Delta G_{\text{binding}}$ is the binding energy of the dopant in the HfTe2 lattice relative to its pure metal phase: $\Delta G_{\text{binding}} = E(\text{HfTe}_2:\text{M}) - E(\text{HfTe}_2) - E(\text{M}_{\text{bulk}})$.
- *n* is the number of electrons transferred in the dissolution reaction (taken as the common oxidation state) .
- *F* is the Faraday constant (conversion: 1 eV = 96.485 kJ/mol).

The results are shown in Table S5.

Table S5. Calculated dissolution potentials (U_{diss}) for key TM-doped $HfTe_2$ systems.

Element	U° (V vs. SHE)	$\Delta G_{binding}$ (eV)	Oxidation state *n*	U_{diss} (V vs. SHE)
Fe	-0.44	+1.487	2	-1.184
Co	-0.28	+1.200	2	-0.880
Ni	-0.25	+1.039	2	-0.770
Ru	+0.45	+0.671	2	+0.114
Re	+0.30	+3.273	4	-0.518
Ir	+1.16	+1.023	3	+0.819
Au	+1.50	+0.966	3	+1.178

All U_{diss} values are lower than the corresponding U° because $\Delta G_{binding} > 0$ indicates the dopant is less stable in the $HfTe_2$ lattice than in its pure metal form. The difference $U^\circ - U_{diss} = \Delta G_{binding} / n$ quantifies the stability loss due to lattice incorporation.

Under acidic HER conditions (pH = 0, operating potential ~0 V vs. RHE ≈ 0 V vs. SHE): Fe, Co, Ni, and Re-doped $HfTe_2$ have $U_{diss} < 0$ V, indicating thermodynamic susceptibility to dissolution. Ru-doped $HfTe_2$ has U_{diss} slightly positive (+0.11 V), suggesting marginal stability. Ir and Au-doped $HfTe_2$ maintain positive U_{diss} (+0.82 V and +1.18 V), indicating better resistance to dissolution.

References:

[S1] J. K. Nørskov, J. Rossmeisl, A. Logadottir, L. Lindqvist, J. R. Kitchin, T. Bligaard, Jónsson, *J. Phys. Chem. B* 2004, **108**, 17886–17892.
[S2] J. K. Nørskov, T. Bligaard, A. Logadottir, J. R. Kitchin, J. G. Chen, S. Pandelov, Stimming, *J. Electrochem. Soc*. 2005, **152**, J23–J26.
[S3] X. Yang, L. Lin, X. Guo and S. Zhang, *J. Catal.*, 2024, **435,** 115548.
[S4] X. Y. Guo, S. R. Lin, J. X. Gu, S. L. Zhang, Z. F. Chen and S. P. Huang, *ACS Catal.*, 2019, **9,** 11042–11054.
[S5] A. J. Bard, R. Parsons and J. Jordan, *Standard Potentials in Aqueous Solution*, Marcel Dekker, New York, 1985.